Inertial Instability and Rossby Wave Breaking in a Numerical Model

DONAL J. O'SULLIVAN

Northwest Research Associates, Bellevue, Washington

MATTHEW H. HITCHMAN

Department of Atmospheric and Oceanic Sciences, University of Wisconsin—Madison, Madison, Wisconsin

(Manuscript received 11 March 1991, in final form 15 September 1991)

ABSTRACT

A mechanistic model of the middle atmosphere is used to study the interaction between Rossby waves forced at the extratropical tropopause and inertial instability in the equatorial lower mesosphere. The impact of cross-equatorial shear strength and Rossby wave forcing amplitude is explored. Model results support the hypothesis, based on satellite temperature observations, that Rossby waves organize regions of equatorial inertial instability into coherent large-scale circulations. Horizontal convergence and divergence maxima are found stacked over the boundaries of regions of anomalous potential vorticity (PV). This supports observational diagnoses and theoretical expectations that parcel inertial accelerations arise in regions of anomalous PV, with divergence and convergence occurring at the boundaries. Although cross-equatorial shear determines the initial volume of inertially unstable air, Rossby waves arriving from the winter hemisphere deform PV contours such that zonally confined regions of anomalous PV extend well into the winter hemisphere and somewhat into the summer hemisphere. Significant parcel inertial accelerations are diagnosed to occur in anomalous PV tongues to 30° latitude in the winter hemisphere. Using a smaller cross-equatorial shear delays the penetration of anomalous PV into the winter hemisphere, while increasing the Rossby wave forcing amplitude causes a more rapid evolution of the low-latitude flow.

These results suggest that inertial instability is intimately involved in Rossby wave breaking in the subtropical winter mesosphere. The horizontal scales of inertially unstable regions coevolve with those of PV anomalies, and so affect the breaking process from inception. The vertical scale of inertial circulations is much smaller than that of Rossby waves; hence, Rossby wave PV anomalies are eroded by vertical mixing as well as horizontal mixing. Gravity waves radiate away from the inertially unstable regions, which effectively convert energy from rotational to divergent modes. The interplay between inertial and gravitational instabilities and their role in causing irreversible mixing in the winter subtropics is explored. The effects of inertial instability on the seasonal evolution of PV is discussed from the point of view of "PV thinking."

1. Introduction

Extratropical planetary Rossby waves are known to propagate energy upward and equatorward from their tropospheric source region. Much of this wave activity reaches the equatorial middle atmosphere, where relatively little is known about its fate. Data from the Limb Infrared Monitor of the Stratosphere (LIMS) experiment revealed that, during the northern winter 1978/79, vertically layered, large-scale temperature perturbations ("pancake structures") appeared in the tropics (Hitchman et al. 1987). An example is shown in Fig. 1. Their occurrence in altitude, latitude, and time was limited by the distribution of anomalous potential vorticity (negative inertial stability). Within this region, however, pancake structures were observed only when the subtropical mesosphere was strongly perturbed by stationary Rossby waves of zonal wavenumber 1 and 2. This fact, together with the absence of zonal propagation, led Hitchman et al. to hypothesize that Rossby waves organize inertial accelerations such that they yield coherent, quasi-stationary, persistent circulations detectable by satellite. In Fig. 1, note the similarity in horizontal scale and the phase relationship between the Northern Hemisphere Rossby wave and the tropical stacked features. The Rossby wave exhibits moderate westward tilt with altitude and northeast–southwest phase tilt, indicating upward and equatorward propagation of Rossby wave activity.

Zonally asymmetric meridional circulations in the presence of strong cross-equatorial shear have been diagnosed in a numerical model by Hunt (1981), who attributed their existence to inertial instability. Hunt pointed out that the tropical features were coherently related to the extratropical disturbances in the model. Inertial instability is expected to be a robust feature in most three-dimensional middle-atmosphere models, since they are formulated in the primitive equations,

Corresponding author address: Dr. Matthew H. Hitchman, Department of Atmospheric and Oceanic Sciences, University of Wisconsin—Madison, 1225 W. Dayton Street, Madison, WI 53706.

© 1992 American Meteorological Society

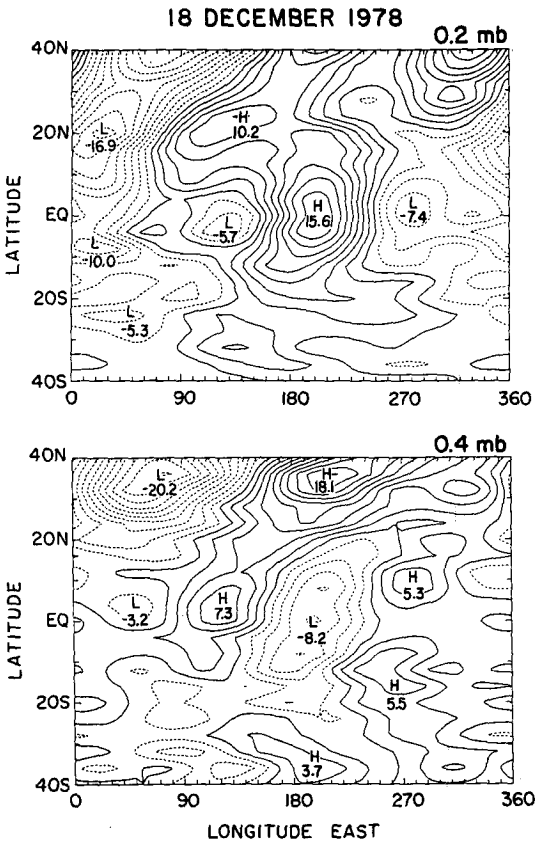

FIG. 1. Plan views of LIMS temperature waves 1–3 at 0.2 mb and 0.4 mb on 18 December 1978, contour interval: 2 K; taken from Hitchman et al. (1987).

which support such motions. Nevertheless, to our knowledge, no one has undertaken a systematic numerical study of the relationship among inertial instability of the basic state, forced Rossby waves propagating into the region, and their interaction with inertial circulations.

Our results show that irreversible mixing of potential vorticity (PV) associated with "Rossby wave breaking" in the vicinity of low-latitude critical surfaces (McIntyre and Palmer 1984) is enhanced by meridional circulations caused by inertial instability. Previous mechanistic studies of Rossby wave breaking have been carried out with models having high horizontal resolution but only one layer in the vertical (e.g., the shallow-water model of Juckes and McIntyre 1987, and the equivalent barotropic model of Salby et al. 1990). One-layer models are not capable of representing meridional overturning associated with inertial instability.

This paper presents initial results from an ongoing study of two numerical models: a mechanistic model developed by Dr. R. Young at NASA Ames Research Center (see Young and Villere 1985), which we have modified into a mechanistic middle-atmosphere model, and the National Center for Atmospheric Research Community Climate Model (NCAR CCM). Here we present results from runs with the Young and Villere model. In section 2 we briefly describe the model characteristics and three useful model diagnostics: potential vorticity, horizontal convergence, and parcel acceleration coefficient. In section 3 several model runs at different horizontal truncation and wave forcing are compared, where cross-equatorial shear of the basic-state zonal wind, $\partial\bar{u}/\partial y$, is moderately large. The evolution of potential vorticity and convergence fields illustrates the interaction between Rossby wave breaking and inertial instability. In section 4 the effect of reducing $\partial\bar{u}/\partial y$ by a factor of ~ 2 is explored. A discussion of the relationship between parcel instability and Rossby wave breaking is given in section 5. The seasonal changes in the distribution of PV are also described, with attention to regions of anomalous PV. We have not yet fully explored the important relationship among convection, inertial circulations, vertical diffusive processes, and model vertical resolution. Those results will be reported separately.

2. Model and diagnostics

The primitive equation model used here is a modification of that used by Young and Villere (1985). As modified, the model extends from 250 mb to 0.02 mb (approximately 10 km to 70 km altitude). The vertical log-pressure coordinate has a grid spacing of 3 km. We ran the model with two different horizontal spectral resolutions with trapezoidal truncation. A T10 run includes zonal wavenumbers, m, from 0 to 10 and total wavenumbers, l, from 0 to 20. A T20 run includes $m = 0$–20 and $l = 0$–40. The equivalent grid spacing is approximately 5° latitude by 10° longitude for T10 and 2.5° by 5° for T20. At moderate horizontal resolution the wave breaking process is readily seen (e.g., Robinson 1988). Salby et al. (1990) found little dependence of the large-scale flow field on model resolution during wave breaking.

The effects of subgrid-scale processes were approximated by a horizontal diffusion applied to vorticity, divergence, and temperature of the form $\nu_2\nabla^2$, where $\nu_2 = 10^5\ \mathrm{m^2\ s^{-1}}$. In addition, dissipation of the form $\nu_6\nabla^6$ was applied to prevent an unphysical accumulation of enstrophy at the smallest scales. For the T10 run $\nu_6 = 2.51 \times 10^{29}\ \mathrm{m^6\ s^{-1}}$, damping the smallest resolvable scale by a factor of e in 1 h, while for the T20 run $\nu_6 = 2.11 \times 10^{28}\ \mathrm{m^6\ s^{-1}}$, damping $l = 40$ by e in 12 minutes. During model integration, zonal-mean zonal winds were relaxed toward 1.5 times the initial state at the rate

$$\alpha(z) = \left[1.5 + \tanh\left(\frac{z - 35}{7}\right)\right] \times 10^{-6}\ \mathrm{s^{-1}}, \quad (2.1)$$

where z is in kilometers, providing a relaxation time scale of ~ 5 days at 60 km. Above 60 km Rayleigh friction of the form

$$\sigma(z) = 10^{-7}\ \mathrm{s}^{-1} + 5 \times 10^{-6}[1 - \exp^{-[(z-60)/20]}]\ \mathrm{s}^{-1} \quad (2.2)$$

was applied to zonal asymmetries to provide a sponge layer, giving a time scale that decreases from ~115 days at 60 km to ~6 days at 70 km. No vertical diffusion or convective adjustment was applied. Differential temperature advection associated with inertial circulations may lead to $\partial\theta/\partial z < 0$. Although vertical accelerations are not explicitly calculated in a primitive equation model, this condition can affect other aspects and may lead to computational instability.

The initial zonal-mean zonal winds were designed to simulate observed cross-equatorial shears near the stratopause during the northern winter solstice. Observations indicate that near solstice $\partial\bar{u}/\partial y$ is substantial, reaching maximum values of ~5 day^{-1} in the equatorial lower mesosphere (Hitchman and Leovy 1986, hereafter HL). Figure 2 shows latitudinally smoothed profiles of $\bar{u}$ and $f - \partial\bar{u}/\partial y$ at 0.4 mb (~55 km altitude) for the period 12–17 December 1978 taken from HL. Between 10°S and 40°N the average value of $\partial\bar{u}/\partial y$ is ~2 day^{-1}. Runs were performed with initial weak or strong cross-equatorial shear of the basic state, with run names distinguished by the suffix W or S. The weak case, $\bar{u}_W$ (shown in Fig. 8a), has contributions corresponding to the subtropical jet, polar night jet, and the quasi-biennial oscillation (QBO):

$$\bar{u}_W = \bar{u}_{ST} + \bar{u}_{PN} + \bar{u}_{QBO}. \quad (2.3)$$

The subtropical jet portion takes the form

$$\bar{u}_{ST} = \sin\left(\frac{90-\phi}{60}\right)\left[\mathrm{sech}\left(\frac{30-\phi}{14}\right) + 1.5\ \mathrm{sech}\left(\frac{-(\phi+40)}{14}\right)\right]e^{-[(z-13)/7]^2} \times 30\ \mathrm{m\ s}^{-1}, \quad (2.4)$$

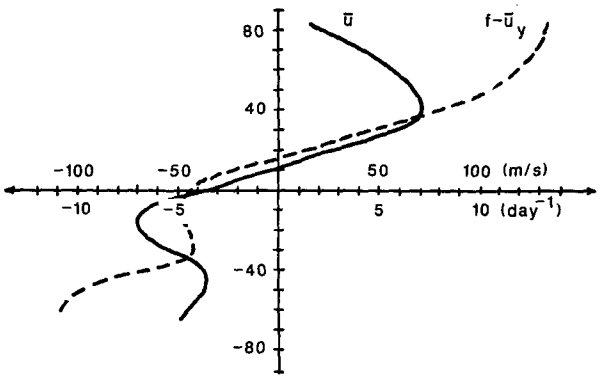

FIG. 2. Latitudinal variation of $\bar{u}$ and $f - \partial\bar{u}/\partial y$ near solstice in the lower mesosphere for northern winter. The hand-smoothed data were taken from the 0.4-mb level winds calculated in Hitchman and Leovy (1986) averaged over the period 12–17 December 1978. Note the region of anomalous PV in the winter subtropics.

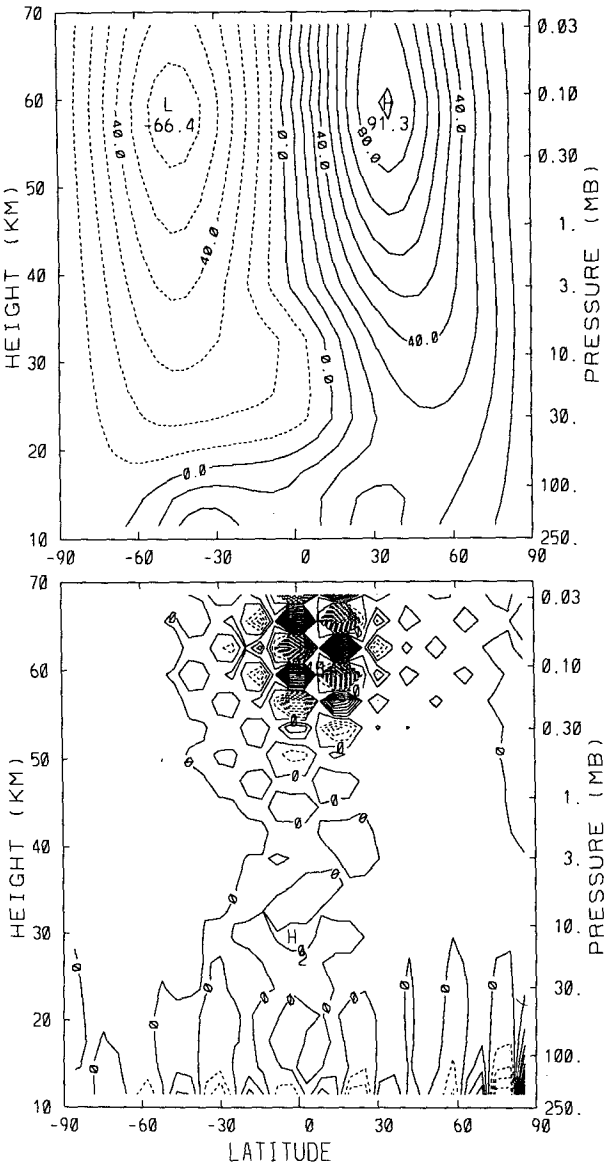

FIG. 3. Latitude–altitude sections of zonal-mean zonal wind (upper, contour interval 10 m s^{-1}) and convergence of the meridional wind (lower, contour interval 1.0×10^{-7} s^{-1}) on day 20 of run T10.0.S.

where ϕ is latitude in degrees and z is altitude in kilometers. This provides a cross-equatorial shear of ~1 day^{-1}. The polar night jet portion is

$$\bar{u}_{PN} = [e^{-[(90-\phi-\phi_0(z))/30]^2} - e^{-[(\phi-45)/25]^2}]\mathrm{UZ}, \quad (2.5)$$

where UZ = 10 m s^{-1} + $z \times 1$ m s^{-1} km^{-1} for $z \leq 60$ km, UZ = 10 m s^{-1} + $(120 - z) \times 1$ m s^{-1} km^{-1} for $z > 60$ km, and $\phi_0(z) = 50 + 9\ \tanh[(z - 40)/12]$ cause the winter westerly jet to trend equatorward with increasing altitude. The QBO portion is taken to be in its easterly phase:

$$\bar{u}_{QBO} - (20\ \mathrm{m\ s}^{-1})e^{-(\phi/20)^2} \quad (2.6)$$

for $25 < z < 40$ km and $\bar{u}_{QBO} = 0$ otherwise. In the strong shear case, $\bar{u}_S$, shown in Fig. 3a, a subtropical mesospheric westerly jet at 25°N was included:

$$\bar{u}_S = \bar{u}_W + (80 \text{ m s}^{-1})e^{-|(\phi+25)/7|} \times \frac{z}{60 \text{ km}}, \quad (2.7)$$

where z is in kilometers, increasing $\partial\bar{u}/\partial y$ in the tropics near 60 km to ~ 2 day^{-1}.

Extratropical Rossby waves were forced by specifying a zonal wave one geopotential height anomaly at the lower boundary such that $\Phi_B = 0$ for $\phi \leq 30$°N and

$$\Phi_B(\phi, t) = h \sin^2[3(\phi - 60)](1 - \exp^{-t/2.5}) \quad (2.8)$$

for $\phi > 30$°N, where t is in days and $h = 0$, 50, 200, or 300 m. In the model run designation the forcing amplitude follows the truncation. We report on low-truncation runs in the presence of strong shear (T10.0.S, T10.50.S, T10.200.S, T10.300.S). We compare these with two higher-truncation runs, one at 200-m forcing in the presence of strong shear (T20.200.S) and one with 300-m forcing in the presence of weak shear (T20.300.W).

In the experiments described here, a zonal wave one Rossby wave propagates energy upward and equatorward in the Northern Hemisphere, forming a low-latitude critical layer where differential vorticity advection leads to a winding up of PV contours in a process known as wave breaking (McIntyre and Palmer 1984). This quasi-horizontal stirring of air is most easily viewed in the approximately conserved potential vorticity field. Typically this shows a tongue of low or negative PV being wound north and eastward to the north of a comparable tongue of high PV air originally from higher latitudes. The low-latitude Rossby wave breaking occurs in a zone lying to the north of the zonal-mean critical line (O'Sullivan and Salby 1990). In the mesosphere, westerlies extend to near the equator so wave breaking occurs at low northern latitudes. Under such circumstances the quasi-horizontal stirring of air can lead to local inertially unstable conditions by drawing anomalous vorticity across the equator.

The potential vorticity diagnostic used in this study to infer regions of inertial instability and behavior of the Rossby wave disturbance is the "poor man's PV" used by Baldwin and Holton (1988):

$$P^*(x, y, z) = -g[f + \zeta(x, y, z)] \times \left(\frac{-\theta(x, y, z)R}{p(x, y, z)g}\right)\left(\frac{dT}{dZ_{std}}(z) + \frac{g}{C_p}\right) \quad (2.9)$$

where

$$p(x, y, z) = p(z)\left(\frac{\theta(z)}{\theta(x, y, z)}\right)^{\alpha},$$

$$\alpha^{-1} = -\frac{R}{g}\left(\frac{dT}{dZ_{std}}(z) + \frac{g}{C_p}\right),$$

g is the acceleration due to gravity, $\zeta(x, y, z) = \partial v/\partial x - \partial u/\partial y$ is the relative vorticity at the model altitude z in log pressure, f is the Coriolis parameter, R is the gas constant for dry air, $dT/dZ_{std}(z)$ is the vertical temperature gradient of the U.S. Standard Atmosphere at the model altitude, C_p is the specific heat at constant pressure, $\theta(x, y, z)$ is the potential temperature on the model surface, $\theta(z)$ is global mean potential temperature, and $p(x, y, z)$ is the resulting "effective pressure" varying over the model surface at altitude z. Here P^* is defined by values at a given level; no vertical derivatives need be calculated. The variation of static stability is assumed to be due entirely to pressure variations of an isentropic surface. For pancake structures those variations affect P^* in the same sense as variations in $\partial T/\partial z$, so this approximation is qualitatively correct.

Consider linear inertial instability theory, where small parcel excursions do not influence the mass distribution. Generalizing from section 9.1 of Holton (1979), a parcel displaced horizontally a distance δs perpendicular to the regional large-scale velocity vector will accelerate at the rate

$$\frac{\partial^2 \delta s}{\partial t^2} = -f(f + \zeta)\delta s. \quad (2.10)$$

We will refer to $-f(f + \zeta)$ as the acceleration coefficient. When $\zeta = 0$ and the fluid is convectively stable, P^* in (2.9) is negative in the Southern Hemisphere and positive in the Northern Hemisphere, and the acceleration coefficient is negative in both hemispheres, indicating inertial stability. Regions where relative vorticity causes this coefficient to be positive will be referred to as regions of anomalous PV (HL). Inertial instability will occur where P^* is negative in the Northern Hemisphere and positive in the Southern Hemisphere. With any nonzero value of ζ near the equator there will be a region of anomalous PV. In particular, near solstice $\partial\bar{u}/\partial y$ is substantial, reaching maximum values in the lower mesosphere. Anomalous PV is found in the subtropical winter hemisphere, with the region being larger for larger values of shear. In such regions angular momentum increases toward the earth's rotation axis and displaced parcels will accelerate due to inertial instability. The presence of zonal asymmetries, such as those due to planetary Rossby waves, would be expected to alter the locations and extent of regions of anomalous PV. The physical interpretation of the cause of inertial instability in the zonally asymmetric case is that angular momentum about a local vortex increases toward its rotation axis. The vortex may be translating, amplifying, or changing its shape, making specification of the rotation axis difficult in practice. Nevertheless, the instantaneous relative vorticity is well defined.

Zonally symmetric inertial instability occurs in the form of vertically stacked cells of meridionally overturning flow. In the linear limit, inertially driven cir-

culations are confined to where $-f(f - \partial\bar{u}/\partial y) > 0$. Zonally symmetric linear inertial instability theory predicts that, in the absence of vertical diffusion, growth rates will be largest at the smallest vertical scales (Dunkerton 1981; Stevens 1983). In the numerical model the minimum vertical wavelength is constrained to be a two-grid wave vertically ($L_z = 2\delta z$), so this becomes the dominant vertical scale of the instability in these model simulations. Extensions of theory to the zonally asymmetric case have been made by Boyd and Christidis (1982) and Dunkerton (1983).

From linear theory, the dependence of the acceleration coefficient on f implies that in regions of anomalous PV, parcel accelerations will tend to be larger farther from the equator. Large negative values of this coefficient indicate a strong restoring effect due to inertial stability. An e-folding time scale for meridional parcel displacement may be obtained by taking $[-f(f + \zeta)]^{-1/2}$.

Parcels displaced horizontally into a region of anomalous PV will accelerate, leading to local horizontal divergence, while parcels leaving such a region will decelerate, leading to local horizontal convergence. Thus, since the inertial motions are divergent and the Rossby waves primarily nondivergent, horizontal convergence will be used as a diagnostic of the presence of inertial circulations. It will be seen that the convergence pattern for pancake structures is quite distinct from that of Rossby waves or large-scale gravity waves.

All model plan views are cylindrical equidistant projections. The horizontal domain is 90°S–90°N, 0°–360°E.

3. Strong shear case

a. Zonal mean

In the absence of Rossby wave forcing, zonal-mean meridional circulations arise in the presence of nonzero cross-equatorial shear. Figure 3 shows $\bar{u}$ and $-\partial\bar{v}/\partial y$ for case T10.0.S after 20 days of integration. Near 60 km in the tropics, $\partial\bar{u}/\partial y \sim 2.3$ day^{-1}, similar to smoothed shears inferred from the LIMS data shown in Fig. 2. Since $f \sim 2.3$ day^{-1} near 10°N, the region of anomalous PV is bounded by 0° and 10°N. The acceleration coefficient reaches a zonally symmetric positive maximum of $\sim 1.5 \times 10^{-10}$ s^{-2} near 5°N (not shown), corresponding to an e-folding time scale for parcel accelerations of ~ 1 day. From linear theory, meridionally displaced parcels will accelerate upon entering such a region and decelerate upon leaving, yielding patterns of horizontal divergence and convergence centered on the zero PV contours, with largest speeds in between. On day 20 zonal-mean meridional motions exceeding 1 m s^{-1} (not shown) occur in the inertially unstable region, taking the form of stacked cells alternating in sign every other vertical grid point. In this nonlinear numerical solution, convergence and divergence regions maximize near the equator and 20°N with amplitude $\sim 10^{-6}$ s^{-1} (Fig. 3). In the present model, radiative relaxation of the mean state yields values of $\bar{v}$ that are probably much weaker than exist in the middle atmosphere near solstice. In models such as the NCAR CCM, the balance between the detailed radiative code and gravity wave driving is such that stronger parcel displacements would occur due to the zonal-mean circulation.

Surprisingly, no zonally asymmetric features appeared in run T10.0.S. The experiment was repeated with $h = 1$ m, yielding a similar result. The theoretical works of Boyd and Christidis (1982) and Dunkerton (1983) suggest that for the shear values used here, linear growth rates should be largest for planetary-scale zonally asymmetric circulations. Apparently, model diffusion is sufficient to suppress growth of numerical noise in the zonal asymmetries, but not growth of zonal-mean circulations arising from the finite-amplitude zonal-mean meridional flow imposed by radiative relaxation.

Hitchman and Leovy speculated that the mean meridional circulation associated with the semiannual oscillation (SAO) may be accentuated by zonal-mean inertial accelerations. In particular, the sudden amplification of the SAO flow structure in mid-December of 1978 coincided with the appearance of strong $\partial\bar{u}/\partial y$. Observed SAO flow geometry thereafter contained a vertically confined region of strong $\partial\bar{u}/\partial y$ that descended with the layer of maximum easterlies. These model results suggest that zonal-mean meridional motions caused by other processes can indeed be accentuated by inertial accelerations.

The strength and shape of the mean meridional circulation depends somewhat on the magnitude of Rossby wave forcing and on horizontal resolution. Qualitatively, the zonal-mean horizontal convergence patterns are quite similar for the zero forcing run (T.10.0.S), a disturbed run (T10.200.S), and a disturbed run at doubled horizontal resolution (T20.200.S) (not shown). But Rossby wave forcing increases typical values of $-\partial\bar{v}/\partial y$ by a factor of ~ 3. Still larger values are found with higher resolution, despite the slightly larger diffusion used. Rather than indicating truly zonally symmetric overturning, however, these values are zonal means of meridional convergence patterns that vary markedly in longitude.

b. Zonal asymmetries

Plan views of potential vorticity, P^*, and horizontal convergence, $-\nabla \cdot \mathbf{V}$, near 60 km on day 16 of run T10.200.S are shown in Fig. 4. The Southern Hemisphere is filled with easterly flow, negative (normal) values of P^*, and is relatively undisturbed (Fig. 4, upper). By contrast, in the Northern Hemisphere westerlies a quasi-stationary Rossby wave 1 appears as zonal asymmetries in the velocity vectors and P^* contours. North of the equator and south of the zero P^* contour,

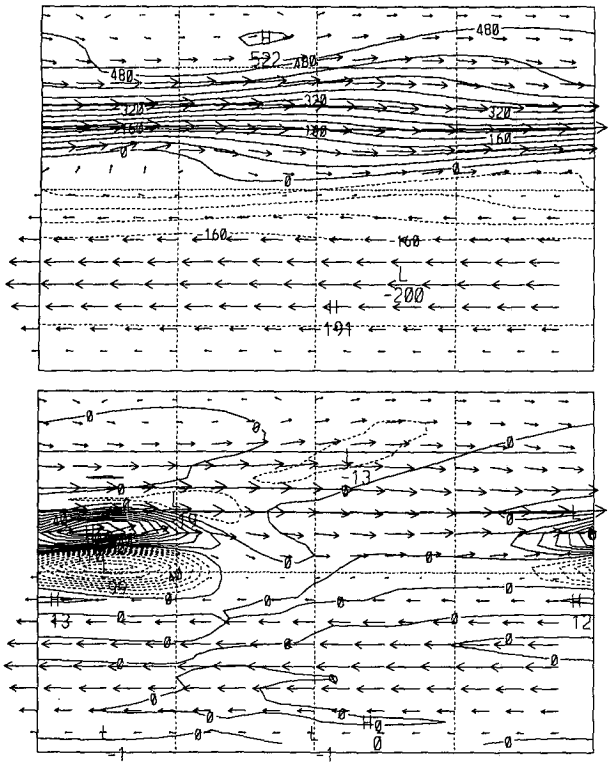

FIG. 4. Plan views of P^* (upper, contour interval 4×10^{-9} K m^2 s^{-1} kg^{-1}) and horizontal convergence (lower, contour interval 1.0×10^{-6} s^{-1}) at level 32 (~0.2 mb) on day 16 of run T10.200.S. Arrows indicate horizontal wind speed and direction. The longest vector is 105 m s^{-1}. The domain is 90°S–90°N, 0–360°E.

the flow is inertially unstable. The zero contour is deformed poleward to almost 20°N near 60°E, with subtropical velocity vectors indicating substantial northward flow across the inertially unstable region at this level. This is reflected in the dominant divergence/convergence pattern in the region 10°S–30°N, 310°E eastward to 110°E in the lower frame of Fig. 4. Thus, a corresponding plot of $-\partial\bar{v}/\partial y$ (e.g., Fig. 8) would be interpreted as a zonal smearing of a concentrated region some 160° longitude wide. Based on this convergence pattern, inertial instability is enhanced where the wave ridge trails southwestward toward the equator and suppressed where the trough reaches the equator. This is compatible with the fact that a ridge contains negative relative vorticity.

The effect of Rossby wave forcing amplitude is seen in Fig. 5. With weak forcing (T10.50.S, Fig. 5, upper), the flow field is dominated by the largest scales, indicative of slower wave breaking. On the same model day, the divergence field in the case of strong forcing (T10.200.S, Fig. 5, lower) contains smaller-scale features and is more turbulent in appearance, suggesting a more advanced stage of wave breaking.

c. *Temporal evolution*

A time sequence of P^* and $-\nabla \cdot \mathbf{V}$ plots near 60 km (Fig. 6) illustrates the relationship between Rossby wave breaking concepts and inertial instability. By day 14 of run T20.200.S a blob of positive P^* near 10°N, 70°E has broken away from the parent body and is surrounded by anomalous PV (Fig. 6a). The corresponding divergence field (Fig. 6b) exhibits an inertial instability signature, with divergence maximizing over the equator and convergence maximizing near the main $P^* = 0$ contour. This divergence/convergence pattern is compatible with what is expected from the northward flow seen in this region. The acceleration coefficient for day 14 near 60 km is shown in Fig. 7. Large accelerations are expected near 20°N, 50°E, evidently contributing to the concentrated convergence region just to the north in Fig. 6b. The maximum of $\sim 10^{-9}$ s^{-2} corresponds to an e-folding time scale of ~0.3 days. By drawing tongues of anomalous PV farther poleward, Rossby waves induce inertial instability of a stronger magnitude than in the symmetric case.

By day 14 there is already evidence that the embedded blob of positive P^* is modifying the shape of the divergence region. Two days later (Fig. 6c) the blob has reconnected to the west and a new tongue is being

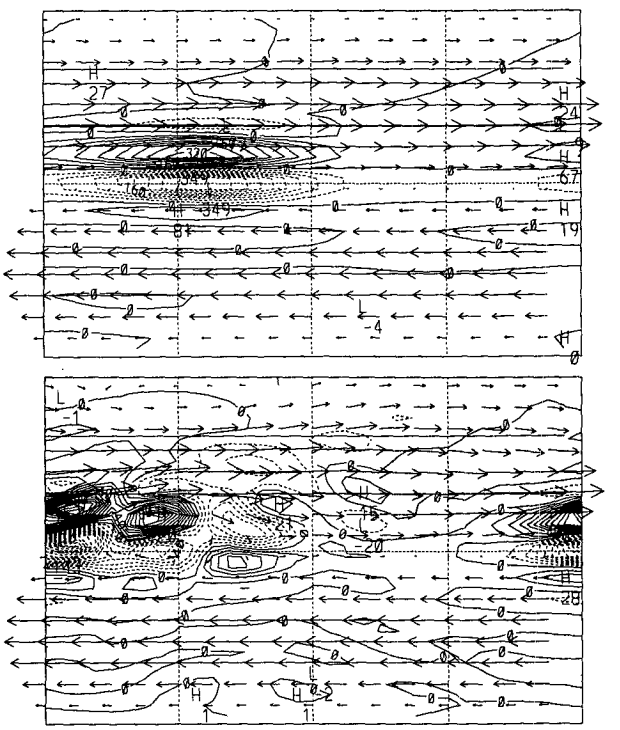

FIG. 5. Horizontal convergence on day 20 of runs T10.50.S (upper, longest vector 94 m s^{-1}) and T10.200.S (lower, longest vector 108 m s^{-1}). In both panels the contour interval is 1.0×10^{-6} s^{-1}.

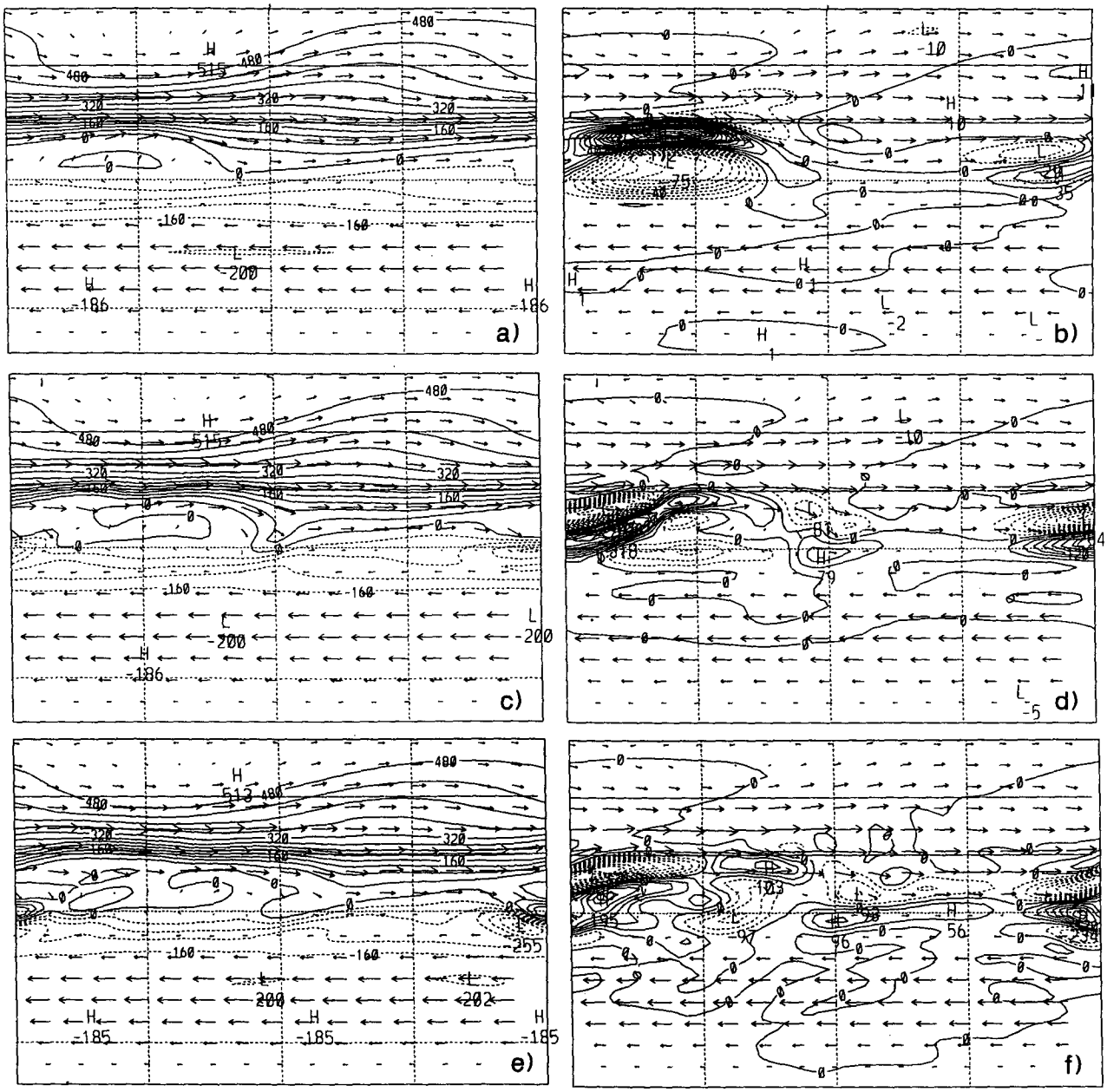

FIG. 6. Potential vorticity (left, contour interval 4.0×10^{-9} K m^2 s^{-1} kg^{-1}) and horizontal convergence (right) for run T20.200.S near 0.2 mb on days 14 (top), 16 (middle), and 18 (bottom). In (b) the contour interval is 1.0×10^{-6} s^{-1} and in (d) and (f) is 3.0×10^{-6} s^{-1}. The maximum horizontal wind speeds are near 115 m s^{-1} in each panel.

drawn across the equator near 180°E. The convergence pattern on day 16 (Fig. 6d) is more complex than before, but again maximum values are found near the boundaries of inertially unstable regions. Note the convergence center arising near 5°S, 180°E centered on the contour of anomalous P^* for the Southern Hemisphere. By day 18 the patterns are even more complex (Fig. 6e,f). The negative P^* anomaly near 10°S, 340°E in Fig. 6e is associated with diabatic vertical motions.

The interaction of the vorticity anomalies associated with the Rossby wave and the positive and negative vortices of the winter and summer hemispheres, respectively, has led to differential vorticity advection and winding up of PV contours. The complex modulation of regions of anomalous PV controls where inertial instability occurs. Four other aspects may also be appreciated. First, if a Rossby wave breaks within ~30° of the equator, motions will be modified by inertial instability. Second, inertial instability is a fast

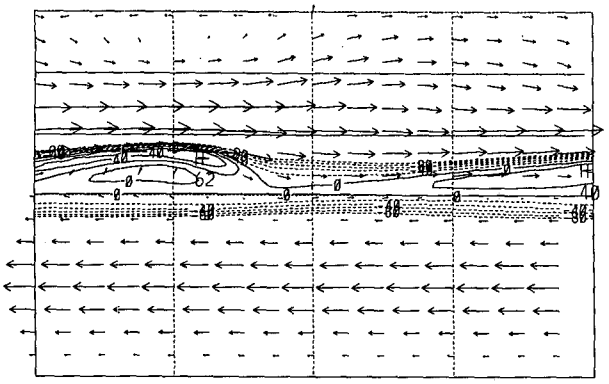

FIG. 7. Coefficient of inertial acceleration on day 14 of run T20.200.S near 0.2 mb [cf. Eq. (2.10)], contour interval 2×10^{-10} s^{-2}.

process. Third, the horizontal scale of the inertially unstable region matches that of the PV anomaly, while the vertical scale is much smaller than that of the PV anomaly. Thus, inertial instability may play a dominant role in causing irreversible mixing in the winter subtropics. Processes such as Kelvin–Helmholtz instability or vertical scale-dependent radiative damping require an enstrophy cascade, together with differential shear in the vertical, to occur before they become effective. Finally, it may be inferred that inertial instability plays a strong role in maintaining the subtropical "surf zone" of weak PV gradient. Rossby waves induce local regions of inertial instability fairly far from the equator, at latitudes where they typically break (cf. Fig. 3b of Baldwin and Holton 1988). In these results circulations associated with inertial instability facilitate the breakup of PV centers, yielding a reduced zonal-mean PV gradient (cf. Figs. 6a,e).

Inertial instability also appears to excite gravity waves, as seen in the Southern Hemisphere in Figs. 5 and 6. In considering the isentropic kinetic energy equations, Silberberg (1991) showed that inertial instability should convert energy from rotational to divergent motions. Stevens et al. (1990) discussed the attainment of a balanced state, involving inertial adjustment in the tropics and geostrophic adjustment in the extratropics. In both cases one would expect gravity waves to emerge as a by-product.

4. Weak shear case

a. Zonal mean

Figure 8 shows $\bar{u}$ and $-\partial\bar{v}/\partial y$ on day 20 for the weak shear case with substantial Rossby wave forcing (T20.300.W). Cross-equatorial shear near 60 km is only about 1 day^{-1}, suggesting a zonal-mean boundary for the inertially unstable region near ~5°N. Yet the zonal-mean divergence pattern extends to 20°N. Again, Rossby waves have distorted the PV contours, organizing regions of inertial instability into local asymmetries that extend farther poleward than the linear zonal-mean criterion would allow.

Although the Rossby wave forcing is larger than in the strong shear case T20.200.S, $-\partial\bar{v}/\partial y$ is typically much weaker. This does not necessarily imply, however, that the total interhemispheric mass transport by inertial accelerations is controlled more by the strength of cross-equatorial shear than by Rossby wave amplitude, since zonal averaging will cancel out large transports of opposing sign in different longitude bands. The dipole in $-\partial\bar{v}/\partial y$ near 40 km, 60°N occurs in the "saddle" of $\bar{u}$ and is compatible with the transient de-

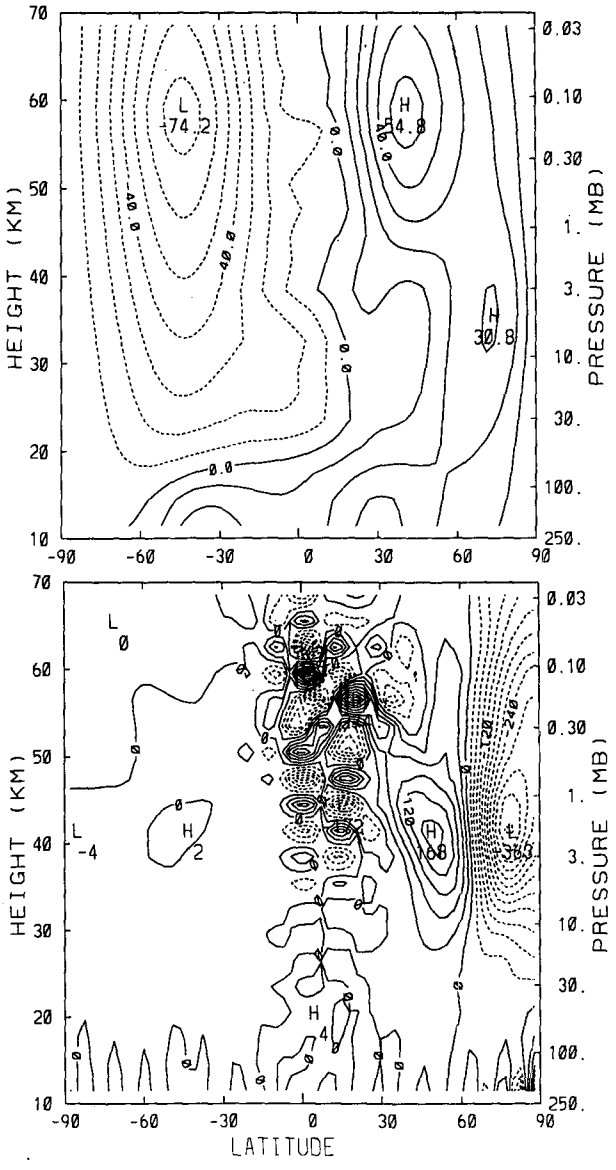

FIG. 8. Latitude–altitude sections of zonal-mean zonal wind (upper, contour interval 10 m s^{-1}) and convergence of the meridional wind (lower, contour interval 3.0×10^{-7} s^{-1}) for run T20.300.W on day 20.

velopment of a minor polar warming event in response to the Rossby wave forcing. It is not directly related to the inertial instability occurring in the tropics.

b. Flow evolution

Behavior in the weak shear case (T20.300.W) is shown in Fig. 9. It may be contrasted with the strong shear, weaker Rossby wave forcing case T20.200.S of Fig. 6. On day 14, convergence magnitudes near the zero PV contour are much smaller in the weak shear case (Figs. 6b, 9b), indicating weaker inertial instability. Moreover, by day 14 wave breaking, in the sense of PV blobs being torn off, has happened in the strong shear, weaker forcing case but not in the weak shear, stronger forcing case, even though PV contours have folded over. This further supports the idea that inertial instability facilitates irreversible deformation and modifies the wave-breaking process. In the weak shear case PV contour windup proceeds farther before inertial instability becomes prominent in the convergence field.

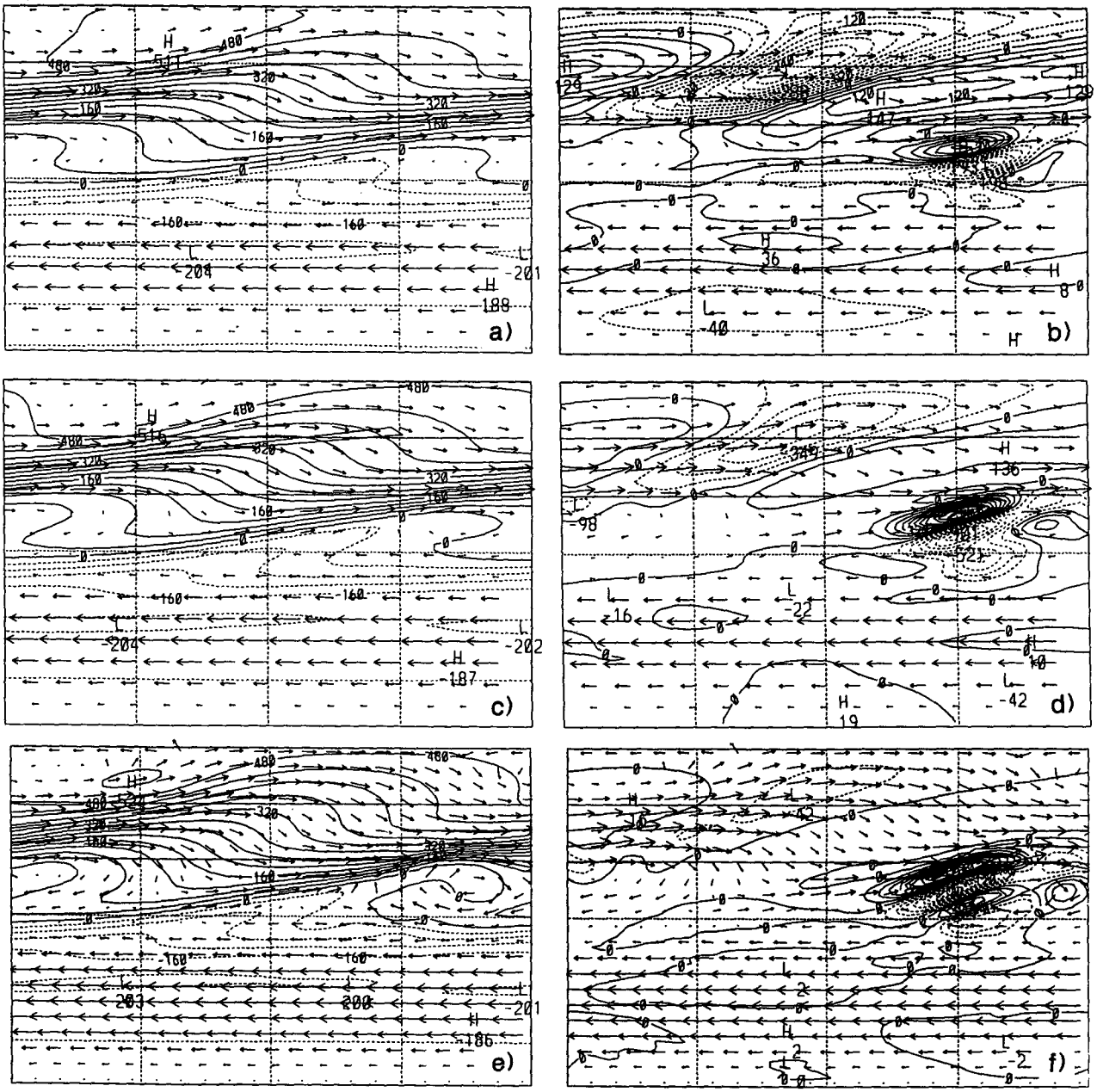

FIG. 9. As in Fig. 6 except for run T20.300.W. In (b) and (f) the contour interval is 3.0×10^{-7} s^{-1}, while it is 8.0×10^{-7} s^{-1} in (d). The maximum horizontal wind speeds are 88 m s^{-1} (top), 89 m s^{-1} (middle), and 100 m s^{-1} (bottom).

Consequently, coherent inertial instability occurs on a finer scale.

Figure 10 shows the inertial acceleration coefficient on day 18 of run T20.300.W (cf. Figs. 9e,f). Substantial inertial accelerations are expected nearly to 30°N in the most poleward extent of the region of anomalous PV. The maximum value is somewhat larger than that seen in the T.20.200.S run shown in Fig. 7. In Fig. 9e the zero PV contour dips south of the equator in a broad band centered near 0°E. The Rossby wave has induced a new region of weakly accelerating parcels in the summer hemisphere (Fig. 10).

Stronger shear enhances inertial instability closer to the equator for smaller Rossby wave amplitudes. A strong Rossby wave in weak shear will cause inertial instability in a more zonally confined region, but with greater meridional extent. Due to this interplay between Rossby wave amplitude and cross-equatorial shear, and due to the meridional tilt of Rossby wave phase axes, it is difficult to predict the longitude band of preferred inertial instability (compare Figs. 7 and 10). Thus, although the Aleutian high is a climatological feature, one cannot infer, a priori, a preferred longitude band of tropical inertial instability and wave breaking.

5. Discussion

a. *Tracer transport and wave propagation*

When low-latitude wave breaking occurs, there is an interaction between the quasi-horizontal folding of potential vorticity and overturning motions driven by inertial instability. The poleward advancing tongue of anomalous PV air creates enhanced inertial instability whose meridional motions have a smaller vertical wavelength than that of the breaking Rossby wave. Consequently, the tongue is pulled poleward or equatorward at alternating levels by the inertial motions. It is noted that this form of stirring is absent in barotropic or equivalent barotropic models, which are sometimes used to study horizontal tracer transport and wave propagation. The inertial instability seen in our 3D model has a vertical wavelength of 6 km, corresponding to an equivalent depth of 37 m (Andrews et al. 1987, p. 180), whereas the barotropic models use an equivalent depth on the order of 10 km. Such large equivalent depths will not permit inertial instability to occur for any realistic distribution of PV. Such models may misrepresent the rate of Rossby wave breaking and subtropical transport. Similarly, cross-equatorial wave propagation in barotropic models (Webster and Holton 1982) may occur more readily by suppression of inertial instability.

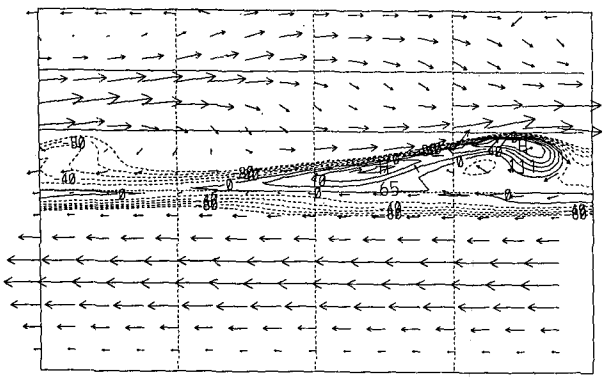

FIG. 10. Coefficient of inertial acceleration on day 18 of run T20.300.W near 0.2 mb [cf. Eq. (2.10)], contour interval 2 $\times 10^{-10}$ s^{-2}.

Rather than tending to dynamical self-preservation, a region of anomalous PV may be regarded as a convective cavity that entrains its surroundings and detrains into its surroundings. Given a zonally symmetric cavity, a Rossby wave may reshape the cavity or can make it larger or more active. Our results show that a Rossby wave may also induce such cavities. Since tracer transport is facilitated by inertial instability, it is significant to note that Rossby waves determine where this occurs. This may be important whether material from one hemisphere mixes uniformly a short distance into the other hemisphere or mixes quite far in one region but not at all elsewhere.

b. *Relationship between inertial and gravitational instabilities*

Consideration of Ertel's potential vorticity shows that there are two types of parcel instabilities: gravitational and inertial (e.g., Andrews et al. 1987). Gravitational instability occurs when potential temperature decreases upward, while inertial instability occurs when angular momentum decreases away from a rotation axis. In an unstable region, parcel motions will act to restore stable gradients of PV. In a particular situation, instability of one type may occur first, which can lead to instability of the other type. Bennetts and Hoskins (1979) studied these instabilities in the context of tropospheric synoptic-scale flows and found that latent heat release is generally required for gravitational destabilization to occur. They argued that purely differential motion is not likely to yield gravitational instability unless net heating or friction creates an inertially unstable configuration of sufficient magnitude. This type of preconditioning does occur in the equatorial middle atmosphere near solstice, with the kinetic energy available in the horizontal shear flow sufficient to overcome resistance to vertical displacements. As has been shown, differential vorticity advection in the horizontal will enhance horizontal shears in the subtropics to the point of inertial instability. If meridional accelerations vary with altitude in a region where θ surfaces are sloped, differential potential temperature advection can lead to $\partial\theta/\partial z < 0$ and gravitational instability. Even if θ surfaces are initially flat, the fact that the region of inertial instability is bounded laterally will assure over-

turning circulations, which can lead to $\partial\theta/\partial z < 0$. Radiative relaxation is insufficient to prohibit this. In the mesosphere, where static stability is somewhat weak, plumes may travel significant distances in the vertical. If convective instability sets in, this will serve to homogenize PV in the overturning cavity, tending toward neutral stability. Convection would thus effectively limit inertial instability. In tropospheric convective complexes, the reverse may occur, where convection can induce a region of inertial instability, which in turn helps homogenize PV.

Since the dry adiabatic lapse rate is 10 K/km, a vertical temperature gradient of -10 K/km would be required locally for convective instability to occur. Figure 11 shows that it is common for the model vertical temperature gradient to approach this value in inertially unstable regions. The largest negative value is ~ -7 K/km near 20°N, 300°E. We hypothesize that inertial and convective instability in the equatorial middle mesosphere help mechanically dissipate Rossby wave activity. This process ought to be parameterized in 2D models of the middle atmosphere that seek to represent the effects of Rossby waves (Hitchman and Brasseur 1988; Garcia 1991). Holton (1983) parameterized the effect of inertial instability on the mean state, but did not couple it with Rossby wave dissipation.

c. *Inertial instability and the solstitial PV distribution*

To the extent that inertial instability modifies Rossby wave breaking, it causes a transport of PV along isentropes toward the summer hemisphere, acting to restore stability in the winter subtropics. Figure 2 indicates typical distributions of $\bar{u}$ and of $f - \partial\bar{u}/\partial y$, which approximately represents the latitudinal variation of PV near the boreal winter solstice. From the point of view of PV thinking, the total PV in a middle atmospheric layer bounded by two isentropic surfaces is zero, and there are no sources and sinks (Haynes and McIntyre 1987, 1990). Thus, seasonal changes in the distribution of PV can occur only by mass dilution or concentration and by along-isentrope transport. Polar cooling during the wintertime leads to isentropes rising in altitude and mass diverging downward out of the layer, with concentrated PV showing up as the westerly polar vortex ($\bar{u}$ decreasing poleward in Fig. 2). Summer heating causes descending isentropes and mass converging upward into the layer, with diluted PV manifested as summer easterlies. To obtain the solstitial tropical PV distribution suggested in Fig. 2, anomalous winter values must come from the summer hemisphere. The latitudinal profile of angular momentum in the free atmosphere departs from a constant value because it is coupled to the ground by vertically propagating, dissipating waves. Thus, any cross-equatorial advection will necessarily lead to finite values of $\partial\bar{u}/\partial y$, hence to regions of anomalous PV (Dunkerton 1989). Largest equatorial values of $\partial\bar{u}/\partial y$ occur somewhat below levels where gravity waves break in midlatitudes, capping the extratropical jets and greatly increasing the summer-to-winter flow (e.g., Leovy 1964; Holton 1983; Hitchman et al. 1989). The resulting along-isentrope advection by the diabatic circulation tends to shift the entire PV pattern toward the winter hemisphere. In the seasonal mean, this transport of anomalous PV into the winter hemisphere must be balanced by dilution and along-isentrope transport of normal PV toward the summer hemisphere. This is accomplished by Rossby wave breaking and inertial instability.

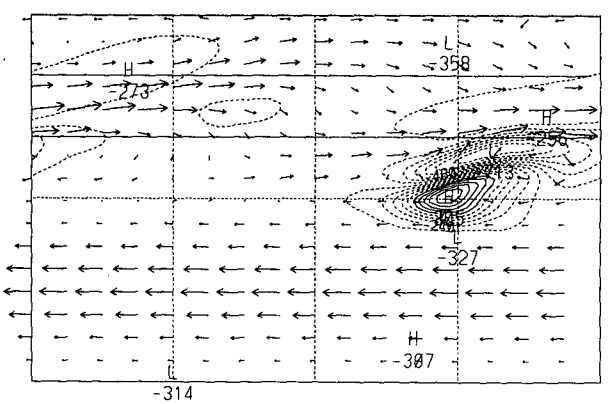

FIG. 11. Plan view of the vertical derivative of temperature at level 31 (~0.2 mb) on day 19 of run T20.300.W, contour interval 6×10^{-4} K m^{-1}.

Acknowledgments. DO'S acknowledges support from NSF Grants ATM-8903282 and ATM-9047965. MHH acknowledges support from NSF Grant ATM-8918574. We would like to thank Francis Bretherton, Tim Dunkerton, John Knox, Conway Leovy, Walter Robinson, and Rich Young for useful conversations. We would especially like to thank Rich Young for providing the model. Computations were performed on computers at the National Center for Atmospheric Research, which is funded by the National Science Foundation.

REFERENCES

Andrews, D. G., J. R. Holton, and C. B. Leovy, 1987: *Middle Atmosphere Dynamics.* Academic Press, 489 pp.

Baldwin, M. P., and J. R. Holton, 1988: Climatology of the stratospheric polar vortex and planetary wave breaking. *J. Atmos. Sci.*, **45**, 1123–1142.

Bennetts, D. A., and B. J. Hoskins, 1979: Conditional symmetric instability—A possible explanation for frontal rainbands. *Quart. J. Roy. Meteor. Soc.*, **105**, 945–962.

Boyd, J. P., and Z. D. Christidis, 1982: Low wavenumber instability on the equatorial beta-plane. *Geophys. Res. Lett.*, **9**, 769–772.

Dunkerton, T. J., 1981: On the inertial stability of the equatorial middle atmosphere. *J. Atmos. Sci.*, **38**, 2354–2364.

——, 1983: A nonsymmetric equatorial inertial instability. *J. Atmos. Sci.*, **40**, 807–813.

——, 1989: Nonlinear Hadley circulation driven by asymmetric differential heating. *J. Atmos. Sci.*, **46**, 956–974.

Garcia, R. R., 1991: Parameterization of planetary wave breaking in the middle atmosphere. *J. Atmos. Sci.*, **48,** 1405–1419.

Haynes, P. H., and M. E. McIntyre, 1987: On the evolution of vorticity and potential vorticity in the presence of diabatic heating and friction or other forces. *J. Atmos. Sci.*, **44,** 828–841.

——, and ——, 1990: On the conservation and impermeability theorems for potential vorticity. *J. Atmos. Sci.*, **47,** 2021–2031.

Hitchman, M. H., and C. B. Leovy, 1986: Evolution of the zonal mean state in the equatorial middle atmosphere during October 1978–May 1979. *J. Atmos. Sci.*, **43,** 3159–3176.

——, and G. Brasseur, 1988: Rossby wave activity in a two-dimensional model: Closure for wave driving and meridional eddy diffusivity. *J. Geophys. Res.*, **93,** 9405–9417.

——, C. B. Leovy, J. C. Gille, and P. L. Bailey, 1987: Quasi-stationary, zonally asymmetric circulations in the equatorial middle atmosphere. *J. Atmos. Sci.*, **44,** 2219–2236.

——, J. C. Gille, C. D. Rodgers, and G. Brasseur, 1989: The separated polar winter stratopause: A gravity wave driven climatological feature. *J. Atmos. Sci.*, **46,** 410–422.

Holton, J. R., 1979: *An Introduction to Dynamic Meteorology, 2d ed.* Academic Press, 391 pp.

——, 1983: The influence of gravity wave breaking on the general circulation of the middle atmosphere. *J. Atmos. Sci.*, **40,** 2497–2507.

Hunt, B. G., 1981: The maintenance of the zonal mean state of the upper atmosphere as represented in a three-dimensional general circulation model extending to 100 km. *J. Atmos. Sci.*, **38,** 2172–2186.

Juckes, M. N., and M. E. McIntyre, 1987: A high-resolution one-layer model of breaking planetary waves in the stratosphere. *Nature,* **328,** 590–596.

Leovy, C. B., 1964: Simple models of thermally driven mesospheric circulation. *J. Atmos. Sci.*, **21,** 327–341.

McIntyre, M. E., and T. N. Palmer, 1984: The "surf zone" in the stratosphere. *J. Atmos. Terr. Phys.*, **46,** 825–849.

O'Sullivan, D. J., and M. L. Salby, 1990: Coupling of the quasi-biennial oscillation and the extratropical circulation in the stratosphere through planetary wave transport. *J. Atmos. Sci.*, **47,** 650–673.

Robinson, W. A., 1988: Irreversible wave–mean flow interactions in a mechanistic model of the stratosphere. *J. Atmos. Sci.*, **45,** 3413–3430.

Salby, M. L., D. O'Sullivan, R. R. Garcia, and P. Callaghan, 1990: Air motions accompanying the development of a planetary wave critical layer. *J. Atmos. Sci.*, **47,** 1179–1204.

Silberberg, S. R., 1991: *The Rotational and Irrotational Kinetic Energy Balance in Isentropic Coordinates During the Global Weather Experiment Boreal Winter.* Ph.D. dissertation, University of Wisconsin–Madison, 211 pp.

Stevens, D. E., 1983: On symmetric stability and instability of zonal mean flows near the equator. *J. Atmos. Sci.*, **40,** 882–893.

——, H.-C. Kuo, W. H. Schubert, and P. E. Ciesielski, 1990: Quasi-balanced dynamics in the tropics. *J. Atmos. Sci.*, **47,** 2262–2273.

Webster, P. J., and J. R. Holton, 1982: Cross-equatorial response to middle latitude forcing in a zonally varying basic state. *J. Atmos. Sci.*, **39,** 722–733.

Young, R. E., and G. L. Villere, 1985: Nonlinear forcing of planetary scale waves by amplifying unstable baroclinic eddies generated in the troposphere. *J. Atmos. Sci.*, **42,** 1991–2006.